The 2009 IEEE/RSJ International Conference on
Intelligent Robots and Systems
October 11-15, 2009 St. Louis, USA

Navigating a Smart Wheelchair with a Brain-Computer Interface Interpreting Steady-State Visual Evoked Potentials

Christian Mandel, Thorsten Lüth, Tim Laue, Thomas Röfer, Axel Gräser, and Bernd Krieg-Brückner

Abstract— **In order to allow severely disabled people who cannot move their arms and legs to steer an automated wheelchair, this work proposes the combination of a non-invasive EEG-based human-robot interface and an autonomous navigation system that safely executes the issued commands. The robust classification of steady-state visual evoked potentials in brain activity allows for the seamless projection of qualitative directional navigation commands onto a frequently updated route graph representation of the environment. The deduced metrical target locations are navigated to by the application of an extended version of the well-established Nearness Diagram Navigation method. The applicability of the system proposed is demonstrated by a real-world pilot study in which eight out of nine untrained subjects successfully navigated an automated wheelchair, requiring only some ten minutes of preparation.**

I. Introduction

People who are severely disabled, quadriplegics in particular, may not be able to comfortably control an electric wheelchair and are thus confined to a push-chair, relying on external help. Here, the research area of human-robot interaction (HRI) can help by providing sophisticated interface techniques. General literature overviews [1], [2] list at least 45 research projects that aim at the development of smart wheelchairs. Many of these projects support specialized input methods that allow the paraplegic to control his or her vehicle without a standard joystick. Common approaches are *Natural Language Communication* [3], [4], *Head Posture Interpretation* [5], [6], and recently the application of *Brain-Computer Interfaces (BCI)*.

A BCI system analyzes specific patterns in the user's brain activity and translates them into commands to control soft- or hardware devices [7]. The principal goal of BCI research is to provide severely disabled people a form of communication which varies from spelling applications [8], [9] to complex rehabilitation systems [10], or prostheses [11]. Navigating a wheelchair with the help of a BCI is a recently grown area in the BCI community. Starting from the idea of manipulating smart environments [12], a person can move a wheelchair to a predefined goal position by using a BCI [13]. But also a low-level navigation of a wheelchair is possible with a limited number of commands [14]. The connection of an SSVEP (steady-state visual evoked potential) based BCI that supports many more commands (13 commands reported in [15]) to a wheelchair has not yet been demonstrated. This work describes the control of the Bremen Autonomous Wheelchair *Rolland* using the SSVEP-based *BremenBCI*.

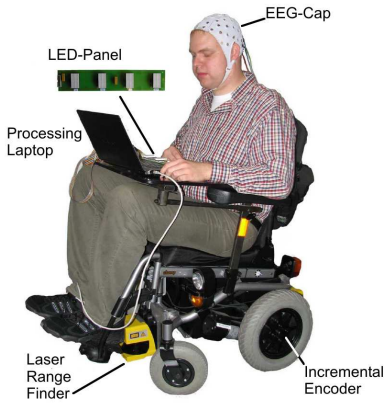

Fig. 1. A person wearing an EEG-cap and navigating the Bremen Autonomous Wheelchair *Rolland*. The system comprises the wheelchair's sensorial equipment, an LED-panel generating the visual stimuli, an EEG-Cap connected to a medical signal amplifier, and a processing laptop.

The remainder of the paper is structured as follows: Section II gives an overview of the system's components, including the hardware modules and the software modules involved. Section III continues with the physiological background of steady-state visual evoked potentials and the EEG signal processing structure to handle nuisance components in EEG data and to classify the desired frequency. Section IV follows with a presentation of the Voronoi graph as the fundamental spatial representation for describing the environment and its embedded navigable paths. Afterwards, Sections V and VI illustrate the path selection scheme applied as well as the extended version of the Nearness Diagram Navigation approach employed. Finally, Section VII presents the results and a discussion of an experimental pilot study that supports the essential ideas of this work.

II. System Overview

With an electrical wheelchair that comprises autonomous navigation capabilities, and an EEG-based HRI that interprets

This work has been partially funded by the European Commission in context of the *6th Framework Programme for RTD* with reference to i) the *SHARE-it project* under contract number FP6-045088, and ii) a *Marie Curie Transfer of Knowledge Fellowship* under contract number MTKD-CT-2004-014211, and by the Deutsche Forschungsgemeinschaft in the context of the SFB/TR8 "Spatial Cognition".

C. Mandel is with the Department of Mathematics and Computer Science – FB3, University of Bremen, PO Box 330440, 28334 Bremen, Germany cmandel@uni-bremen.de

T. Laue, T. Röfer, and B. Krieg Brückner are with the German Research Center for Artificial Intelligence, Research Group: Safe and Secure Cognitive Systems, 28359 Bremen, Germany {tim.laue,thomas.roefer,bernd.krieg-brueckner}@dfki.de

T. Lüth, and A. Gräser are with the University of Bremen, Institute of Automation, 28359 Bremen, Germany {thorsten.lueth,ag}@iat.uni-bremen.de

SSVEPs, this work introduces a complete navigation solution for the paraplegic.

A. The Wheelchair

Serving as the experimental platform, the Bremen Autonomous Wheelchair *Rolland* (cf. Fig. 1) is based on the battery-powered wheelchair Meyra Champ 1.594. Rolland has a differential drive in the back and passive castor wheels in the front. It is equipped with two laser range finders that sense nearby obstacles in a height of about 12cm. The system also provides two incremental encoders which measure the rotational velocities of the two independently actuated rear wheels, allowing for odometric pose estimations. The software architecture used to control Rolland is based on the framework of the GermanTeam [16]. In its version for Rolland, the system embeds all navigational software modules necessary, ranging from the acquisition and maintenance of local and global spatial representations, to high-level path selection, and low-level obstacle avoidance.

B. The Safety Layer

Since the navigation method employed (cf. Section VI) is heuristic in nature, it cannot guarantee collision-free motion. Hence, the wheelchair is equipped with a *safety layer* that ensures that the vehicle will stop in time before a collision can occur. 30 times per second, the safety layer makes a binary decision. Either the current driving command is safe, and it can be sent to the wheelchair, or it is not, and the wheelchair has to stop instead. "Safe" means that if a stop command would be initiated in the next processing cycle (i.e. 33 ms later), the wheelchair would still be able to stop without a collision. Otherwise, it has to be stopped in this cycle, because in the next cycle it would be too late. Whether the wheelchair can stop in time depends on the actual speeds of the two drive wheels and the current drive command, because it will influence the current speeds in the future, the shape of the wheelchair, and its current surroundings. The surroundings are measured using the laser scanners and a model of the environment is maintained in a local obstacle map (cf. Section IV), treating stationary and moving obstacles as equal. Based on the current speeds and the commanded speeds, a *safety area* is searched for obstacles in the map. If the safety area is free of obstacles, the current driving command is safe. Since the shape of such a safety area is rather complex, a large number of safety areas were pre-computed and stored in a lookup table. Two such safety areas are shown in Fig. 3 (the wheelchair turns to the left) and in Fig. 4(b) (the wheelchair drives straight ahead).

C. The BCI System

The stimulus for the SSVEP-based BremenBCI is implemented as an LED-panel of four different diodes oscillating with different frequencies. These diodes relate to the commands chosen to navigate the wheelchair (13 Hz = left, 14 Hz = right, 15 Hz = front and 16 Hz = back). A given command is not interpreted as an ongoing movement waiting for a *stop* command, i.e. the wheelchair stops itself after reaching a nearby target position. Therefore and because of the safety layer, an explicit *stop* command is not required. The software structure of the BCI corresponds to the usual signal processing structure of data acquisition, preprocessing, feature extraction, classification, and application interface. For data acquisition, an electroencephalography (EEG) cap with non-invasive electrodes placed on the scalp is used. The signal is amplified with a *gUSBamp* biosignal amplifier from *g.tec* already equipped with an analog-to-digital converter. The TCP/IP protocol is used as the application interface.

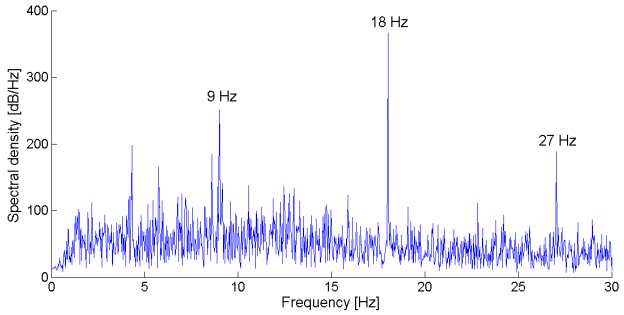

Fig. 2. Typical SSVEP response of an EEG signal acquired during visual stimulation with a flickering frequency of 9 Hz. High peaks at the stimulus frequency and two harmonics are observable in the spectral density of the frequency spectrum.

III. Steady-State Visual Evoked Potentials

Electrical potential changes in brain activity due to an external stimulus are known as evoked potentials (EP) and can be observed in the sensor cortex of the brain. Steady-state visual evoked potentials (SSVEP) are periodic components of the same frequency as a continuously blinking visual stimulus (higher than 4 Hz), as well as a number of harmonic frequencies that can be obtained in brain activity in the visual cortex, when a person is focusing on that stimulus [17], [18]. The SSVEP response can be detected quite robustly, because its characteristic varies from spontaneous brain activity. The strongest response is measurable for stimulation frequencies in the range of 5 - 20 Hz [19]. Figure 2 shows a typical SSVEP response in the visual cortex for a test person focusing on a flickering stimulus of 9 Hz. Peaks at the fundamental frequency as well as two harmonics are observable.

A. Combining Electrode Signals into Channel Signals

We consider visual stimulation with a flicker frequency of fHz. If a person is focusing attention on that stimulus, the SSVEP response in the EEG signal measured as the voltage between a reference electrode and the electrode number i can be estimated as:

$$y_i(t) = \sum_{k=1}^{k=N_h} (a_{i,k} sin(2\pi kft + \Phi_{i,k})) + b(t) \qquad (1)$$

where $0 \leq t < TS$, b describes the noise, TS is the time segment, N_h is a number of harmonics. Each sinusoid on each electrode has its own amplitude ($a_{i,k}$) and phase ($\Phi_{i,k}$).

The nuisance signals b can have several origins: the environment and its effect on the subject, a natural physical

disturbance such as other brain processes, and noise of each electrode on the cap. Therefore, one goal is to magnify the SSVEP response and to decrease the noise to improve the detection of the desired frequency.

A channel s is used as a linear combination of the signals measured by the N_y electrodes. With $0 \leq l < N_s$ and N_s is the number of channels, s is defined by:

$$s_l(t) = \sum_{i=1}^{N_y} w_{i,l} y_i(t) \tag{2}$$

For a channel, the information from the electrodes is resumed in a single scalar at a time t. For the EEG signal processing, the first goal is to find an optimal set $w_{i,l}$, $1 \leq i < N_y$.

For the creation of a single or several channel signals, the minimum energy combination [20] is used in this paper. This method allows the combination not only of pairs or groups of electrodes but also of an arbitrary number of electrodes that cancel the noise as much as possible. The advantage of this method is that the number of electrodes does not need to be chosen beforehand. Its good performance was validated in different applications [21], [22].

B. Feature Extraction and Frequency Classification

For the detection of the stimulus frequencies in the acquired data, the total power $\hat{P}$ at the SSVEP frequency is estimated. SSVEP stimulation frequencies and its harmonics do not always coincide with the Discrete Fourier Transform (DFT). Therefore, slightly different to the squared DFT magnitude, a more general formula that can estimate the power in any frequency is taken into account for estimating the power in the kth SSVEP harmonic frequency in the lth channel signal s_l. With X_k is an SSVEP model (excluding the noise) for each harmonic frequency according to equation 1, the power is estimated to:

$$\hat{P}_{k,l} = \|X_k^T s_l\|^2 \tag{3}$$

After the power of each stimulus frequency is calculated in the acquired brain activity, we use a linear classifier to classify the frequency the subject is focusing on. To consider a stimulus frequency as the desired one and therefore to generate a new command, the corresponding power of that frequency has to exceed a threshold. If more than one power exceeds the threshold, the frequency with the highest power is classified.

IV. Representing Spatial Environments: Route Graphs

The basic representation of the environment, the so-called *evidence grid* [23], is a two-dimensional array of cells each of which stores the evidence that the corresponding location in the environment is occupied by an obstacle. The current implementation maintains a $7.5 \times 7.5 m^2$ grid out of 300×300 cells resulting in a spatial resolution of $2.5 \times 2.5\text{cm}^2$. In definition (4) $EGC(x, y) = 0$ denotes a surely unoccupied, and $EGC(x, y) = 1$ a surely occupied cell respectively.

$$EGC : \mathbb{N} \times \mathbb{N} \rightarrow [0...1] \tag{4}$$

The so-called *distance grid* is derived from the evidence grid and contains the distance to the closest obstacle for each cell. It is calculated by a fast double sweep-line algorithm [24] that computes for each free cell the metric distance to the next occupied cell. Formally it consists of cells as defined in (5), where c is the resolution of the grid, i.e. 2.5cm.

$$\begin{aligned} &DGC : \mathbb{N} \times \mathbb{N} \rightarrow \mathbb{R} \\ &DGC(x, y) = \min_{x', y' : EGC(x', y') > 0.5} c \left| \begin{pmatrix} x - x' \\ y - y' \end{pmatrix} \right| \end{aligned} \tag{5}$$

The final stride in the line of spatial representations is an instantiation of the *route graph* concept [25], [26]. A route graph is a multi-layered and graph-structured representation of the environment in which each graph layer describes the workspace on a different level of abstraction. For this work the route graph comprises a single graph layer, the so-called *Voronoi graph* $\mathcal{VG}$ (7). Its construction is directly based on the distance grid. In a first step, the algorithm computes for every $DGC(x, y)$ whether the distance between two of its generating points, e.g. the occupied cells $EGC(x', y')$ and $EGC(x'', y'')$ that gave $DGC(x, y)$ its value, is greater than a given threshold ϵ. In the formal definition of the resulting *Voronoi diagram* VD (6), the constant value ϵ determines the minimal free space that is required to mark a region as navigable. We use $\epsilon = 70$cm, i.e. the wheelchair's maximal width plus 6cm. Note that the evidence grid, the distance grid, and the voronoi diagram are updated at the same frequency as the safety layer, i.e. every 33ms.

$$\begin{aligned} VD \models \left\{ (x, y) \;\middle|\; \begin{array}{c} x, y \in \mathbb{N}, \exists\, x', y', x'', y'' \in \mathbb{N} : \\ EGC(x', y') > 0.5 \wedge \\ EGC(x'', y'') > 0.5 \wedge \\ d^{x', y'}_{x'', y''} > \epsilon \wedge \\ d^{x,y}_{x', y'} = d^{x,y}_{x'', y''} = DGC(x, y) \end{array} \right\} \\ \text{where } d^{x,y}_{x', y'} = c \left| \begin{pmatrix} x - x' \\ y - y' \end{pmatrix} \right| \end{aligned} \tag{6}$$

The second step searches the Voronoi diagram VD for elements that hold one or more than two neighbors in VD. These cells correspond to terminating or branching nodes respectively, and they are inserted into the Voronoi graph's set of nodes $\mathcal{VG}.N$. The Voronoi graph's set of edges comprises pairs of references to elements in $\mathcal{VG}.N$ that are connected by points out of VD.

$$\begin{array}{lcl} N & \subset & \{(x, y) \mid x, y \in \mathbb{R}\} \\ E & \subset & \{(n^s, n^g) \mid n^s, n^g \in N, n^s \neq n^g\} \\ \mathcal{VG} & \models & (N, E) \end{array} \tag{7}$$

V. Interpreting Qualitative Navigation Commands on Route Graphs

The interpretation of a qualitative driving command such as *go left* basically asks for an adequate projection of the given direction onto the spatial knowledge of the robot. As a primary source of information, this work applies the Voronoi graph $\mathcal{VG}$ for the extraction of the *set of navigable paths* NP(8). In a second step, each path $np \in NP$ is evaluated against the command given, resulting in the best matching path to be forwarded to the local navigation module.

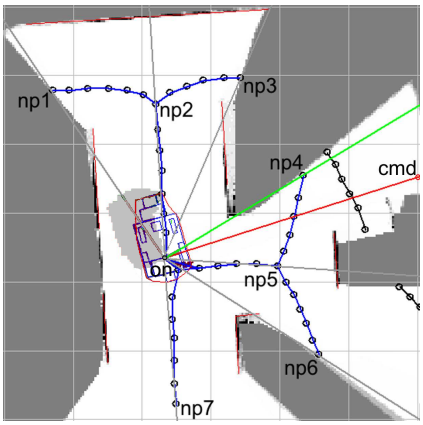

Fig. 3. Assuming a given command $BCI_{cmd} = right$, represented as the vector from on to cmd, the algorithm for the interpretation of qualitative navigation commands (cf. Section V for details) basically evaluates the angle between the vectors $\mid cmd - on \mid$ and $\mid np_j - on \mid$.

$$NP \subset \left\{ np = (e^1, ..., e^i) \;\middle|\; \begin{array}{l} i \in \mathbb{N}, \\ e^1, ..., e^i \in E, \\ e^i.n^g = e^{i+1}.n^s \wedge \\ e^i.n^g \neq e^j.n^s \forall i \geq j \end{array} \right\} \tag{8}$$

In order to derive the set of navigable paths NP from a given Voronoi graph $\mathcal{VG}$, its set of nodes $\mathcal{VG}.N$ is first enriched by the node on, representing the current odometry position. Furthermore, $\mathcal{VG}.E$ is augmented by edges that connect on with all nodes lying in a given circumference of on.

The computation of NP continues by applying an A*-algorithm [27] that searches $\mathcal{VG}$ for all paths that connect on to all other nodes in $\mathcal{VG}.N$, i.e. all possible target positions. The resulting set of paths NP is then filtered for paths the goal of which is not included as an interim node of any other path in NP, with the only exception of paths ending in a branching node with more than two incoming edges. This process leaves NP holding only paths that lead to spatially emphasized target nodes, however covering all in-between goals by the way.

Evaluating each of the navigable paths in NP against a qualitative directional command is a special case of the interpretation of common spatial relations against a given route graph. First described in the context of interpreting coarse verbal route descriptions [4], a qualitative directional command can be given in four different levels of granularity. Due to the limited set of available channels coming from the BCI, i.e. four, we apply a four-valued directional system holding the commands $BCI_{cmd} \in \{front, right, back, left\}$.

$$\begin{aligned} \alpha &= atan2 \begin{pmatrix} np_j.e_i.n^g.y - on.y, \\ np_j.e_i.n^g.x - on.x \end{pmatrix} \mid j \in \{1... \mid NP \mid\} \\ \beta &= \begin{cases} 0 & : \; BCI_{cmd} = front \\ \frac{3}{2}\pi & : \; BCI_{cmd} = right \\ \pi & : \; BCI_{cmd} = back \\ \frac{\pi}{2} & : \; BCI_{cmd} = left \end{cases} \\ score(np_j) &= e^{-\frac{1}{2}\left(\frac{\mid \alpha - \beta \mid}{c}\right)^2} \end{aligned} \tag{9}$$

The final computation of a single path's score is done in two steps. We start by computing the angle α between i) the vector that connects the odometry node on with the goal node $np_j.e_i.n^g$, and ii) the vector that is based in on and aligned to the current heading θ of the wheelchair. Taking the most compatible angle β for the given command BCI_{cmd}, which is $right = 3/2\pi$ in the illustrative example in Fig. 3, and the normalizing constant c, we can now compute $score(np_j)$ as can be seen in (9). With the straightforward maximization of $score(np_j)$ over all $j \in \{1... \mid NP \mid\}$ the algorithm outputs the best matching path, the final node of which is to be forwarded to the local navigation module.

An alternative path selection scheme has been used in [28]. The principle idea is to iterate over the ordered sequence of each navigable path's edges, and to assess the angles between all pairs of consecutive sections. In the case of evaluating a $BCI_{cmd} = front$, a single path's score is formulated as the product over all intermediate scores that state how good two consecutive edges are aligned to each other. The treatment of commands that introduce a bending maneuver, e.g. $BCI_{cmd} = right$, is different because of the additional necessity to choose the best suiting node of a given path for the triggering directional command. The actual approach iterates over all nodes of a path to be evaluated, and calculates for each possible branching node the path's score as the product of scores that arise from the evaluation of $BCI_{cmd} = front$ between all pairs of consecutive edges. The only exception is given by the two sections connected to the selected branching node, where the score's factor is determined by the assessment of the angle between the two edges w.r.t. the given command.

VI. Local Navigation Approach: Nearness Diagram Navigation

Within this work we employ the *Nearness Diagram Navigation (NDN)* approach by Minguez et al. [29], in order to transfer Rolland from its current position to a nearby target position, while avoiding static and dynamic obstacles. The NDN-approach describes the sensor measurements of the visible part of the environment along with the desired target position $p_g = (x_g, y_g)$ as a unique element of an exclusive and complete set of situations. Each of the five situations originally defined is associated with a specific control law that determines the translational and rotational speed to be applied, as well as the desired direction of movement. In order to define a situation, the workspace is divided into sectors centered at the wheelchair's origin. By maintaining a list of distances to the closest obstacles[1] in each of the typically 2° wide sectors, i.e. the nearness diagram (cf. Fig. 4(a)), the system is able to compute free regions in-between two consecutive gaps of the nearness diagram. Finally, a navigable region closest to the goal location is selected.

[1]Actually the NDN-approach not only maintains a list of distances between the surrounding obstacles and the robot's bounding-polygon, but also a list of distances between obstacles and the so-called *safety-zone*. The safety-zone itself is defined by the bounding-polygon plus the constant safety margin D_s.

TABLE I

BASIC NEARNESS DIAGRAM CONTROL LAWS AND SHEER OUT EXTENSIONS

Situation	Direction Of Movement s_θ	Sheer Out Extensions $s_{\theta'}$	Translational Speed v	Rotational Speed ω
HSGR	s_{goal}	$s_{closergap} \pm s_{max}$	$v_{max}\frac{\pi-2\|\theta\|}{\pi}$	$\omega_{max}\frac{2\theta}{\pi}$
HSWR	$s_{goal} \pm \frac{s_{max}}{2}$	–		
HSNR	$\frac{s_{rd}+s_{od}}{2}$	$s_{closergap} \pm s_{max}$		
LS1	$s_{goal} \pm \left(\frac{s_{max}}{2}+\gamma\right)$ where $\gamma = \frac{D_s - D_{sml}}{D_s} \mid (\pi + s_{ml}) - \mid s_{rd} - \frac{s_{max}}{2} \mid\mid$	$s_{ml} \pm s_{safedriveby}$	$v_{max}\frac{D_{obs}}{D_s}\frac{\pi-2\|\theta\|}{\pi}$	
LS2	$\begin{cases} s_{med1} \pm c \text{ if } \mid s_{rd} - s_{med1} \mid < \mid s_{rd} - s_{med2} \mid \\ s_{med2} \pm c \text{ if } \mid s_{rd} - s_{med1} \mid \geq \mid s_{rd} - s_{med2} \mid \end{cases}$ where $s_{med1} = \frac{s_{ml}+s_{mr}}{2}, s_{med2} = \frac{s_{ml}+s_{mr}+n}{2}$	$s_{ml} \pm s_{safedriveby}$		

s_θ $\models$ ND-sector containing the desired direction of movement.
s_{goal} $\models$ ND-sector containing the target p_g.
s_{max} $\models$ Minimal width of a *wide region* in number of ND-sectors.
s_{rd} $\models$ ND-sector with rising discontinuity, i.e. border of the free walking area containing an obstacle that violates the safety-zone.
s_{od} $\models$ ND-sector containing the other border of the free walking area.
D_s $\models$ Safety margin between wheelchair's bounding-polygon and safety-zone.
D_{sml} $\models$ Distance to obstacle in ND-sector s_{ml} that triggered LS1/LS2-situation.
$s_{ml/mr}$ $\models$ ND-sector containing next obstacle left/right of s_{rd}.
$s_{closergap}$ $\models$ ND-sector containing the closer border of the free walking area, i.e. s_{rd} or s_{od}.
$s_{safedriveby}$ $\models$ ND-sector maintaining the minimal tolerable distance to the next obstacle while describing the maximal sheer out direction.
n $\models$ Total number of ND-sectors.
θ $\models$ Direction of movement ($\theta = \pi - 2\pi\frac{s_\theta}{n}$).

This so-called *free walking area* along with its determining obstacles define a specific situation.

In the following we will informally survey necessary conditions for the five basic situations (cf. [30] for a broad analysis). Abbreviations, constant- and variable declarations, as well as the resulting control laws can be found in Table I.

- **H**igh **S**afety **G**oal in **R**egion – The free walking area contains s_{goal}. The closest obstacle to the bounding-polygon does not conflict with the safety-zone.
- **H**igh **S**afety **W**ide **R**egion – The free walking area does not contain s_{goal}. The closest obstacle to the bounding-polygon does not conflict with safety-zone. The width of free walking area exceeds s_{max}.
- **H**igh **S**afety **N**arrow **R**egion – The free walking area does not contain s_{goal}. The closest obstacle to the bounding-polygon does not conflict with safety-zone. The width of free walking area is below s_{max}.
- **L**ow **S**afety **1** – An obstacle conflicts with the safety-zone at the border of the free walking area closest to s_{goal}.
- **L**ow **S**afety **2** – Obstacles conflict with the safety-zone at both sides of the free walking area.

Since Rolland is an example for a non-circularly shaped mobile robot that cannot independently control its kinematic degrees of freedom, i.e. its x- and y-position and its heading θ, the application of the basic NDN-approach has a major drawback. Although sufficient for circular robots being able to turn around their midpoint while entering a narrow passage, the NDN-approach does not model a necessary sheer out movement, needed by vehicles that turn around a point located on their rear axle.

For this reason we have augmented the basic NDN control laws in such a way that they look ahead for upcoming turn maneuvers and initiate a preparatory sheer out movement when necessary (cf. [31] for an in-depth discussion). The most significant advancement is the algorithmic analysis of situations HSGR, HSNR, LS1, and LS2 w.r.t. the *effective width* ew, and the *perspective width* pw of the free walking area (cf. Fig. 4(b) for an example). The situations mentioned are checked for a sufficient width of ew and pw, indicating whether or not a sheer out movement has to be initiated. If necessary, the original direction of movement s_θ is replaced by $s_{\theta'}$, resulting in a temporary circular navigation around s_{rd} (cf. Table I for the sheer out control laws).

VII. EXPERIMENTAL EVALUATION

A. Subjects and Procedure

Nine healthy subjects, between 19 and 38 years old (mean = 26.67), participated in this study. The subjects had different levels of experience in BCI studies. Some of them took already part in earlier BCI studies, while some of them were naive. But none of the subjects had experience in controlling the wheelchair Rolland with or without the BremenBCI. All subjects completed a consent form and a screening questionaire and would have been rejected if they ever had a seizure, epilepsy, mental or physical disorders or skin contact allergies. Table II shows the subjects in terms of age, gender, vision, and experience level in BCI studies.

The SSVEP response in the subject's brain activity was non-invasively acquired with an EEG-cap. The electrodes for data acquisition were placed at sites PO_3, PO_4, O_9, O_{10}, O_z and P_z using the extended 10-20 system of electrode placement [32] with C_z as reference and AF_z as ground. The data was sampled with a sampling frequency $F_s = 128Hz$.

After placing the electrodes, the subject obtained the task to randomly focus attention on each stimulus frequency of the LED panel described in Section II. During this initial task, the threshold for classification of the desired frequency was set individually for each subject. The wheelchair was not moving during the calibration step. Afterwards, a short training phase started. The subject had up to 10 minutes to train the stimulus frequencies and their corresponding commands to navigate the wheelchair, and to become comfort-

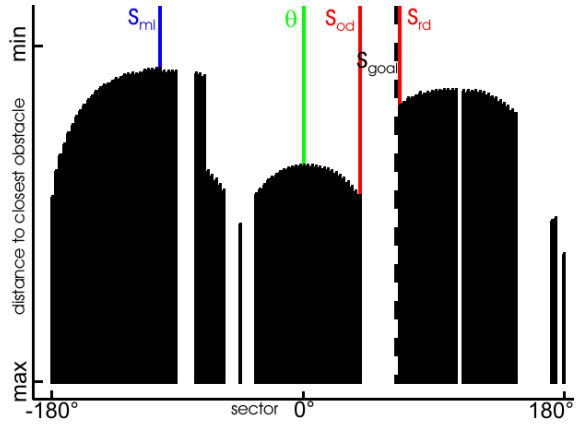

(a) Nearness diagram representation of the environment (cf. Section VI) describing the distances to the closest obstacles.

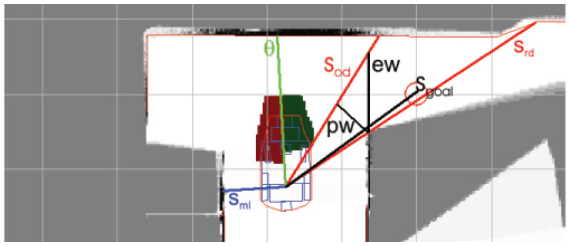

(b) Evidence grid representation of the environment (cf. Section IV) along with a centered and upward facing bounding-polygon of the wheelchair. The target p_g is depicted as a circle.

Fig. 4. Illustration of *Nearness Diagram Navigation* within a simulated environment. S_{od} and S_{rd} denote the left and right border of the free walking area (cf. Section VI), while s_{goal} and θ describe the direction to the local target p_g and the current orientation of the wheelchair respectively.

able with the behavior of the wheelchair when a command was classified. After training, the subject had to navigate the wheelchair Rolland through a course of obstacles. The navigation was expected to be performed in a figure of eight as shown in Fig. 5(a) - 5(b). Starting at position $S = (0, 0)$, the subject had to navigate the wheelchair clockwise around the right obstacle first and then counter-clockwise around the left obstacle. The run ended when the wheelchair reached a point nearby the start position, after navigating through the entire course. Each session consists of up to four runs (depending on the subject).

B. Experimental Setup

In order to compare and evaluate the results of the different experimental runs, a common frame of reference is needed. In our case, this is a global map of the environment, and the ability to localize the wheelchair at any point in time within the map. For creating the map (shown in Fig. 5(a) - 5(b)), we used the *GMapping* implementation from *OpenSLAM* [33]. It is a highly efficient Rao-Blackwellized particle filer that learns grid maps from raw laser range and odometry data [34]. The grid map used for our experiments has a cell size of $2 \times 2\text{cm}^2$ and a total size $14 \times 10\text{m}^2$. Real-time localization during the experimental runs has been realized by a modified version of the GMapping implementation. While leaving the map data untouched, a small number of particles keep track of the wheelchair's position.

TABLE II
SUBJECT INFORMATION

Subject	Gender	Age	Vision	Exp. level
S1	female	26	OK	2
S2	male	38	glasses	1
S3	female	20	OK	0
S4	female	19	OK	0
S5	male	22	OK	0
S6	male	31	OK	0
S7	male	28	OK	2
S8	male	27	OK	2
S9	female	29	OK	1

Experience level:
0 ⊨ Naive in BCI studies
1 ⊨ Participated in a few earlier BCI studies (up to 3)
2 ⊨ Participated in several earlier BCI studies (more than 3)

TABLE III
BCI ACCURACY DURING TRAINING PHASE AND RESULTS OF RUN

Subject	Training	Runs		
	Accur. [%]	Commands	Accur. [%]	Best time [min]
S1	100.00	14.5	100.00	3:37
S2	96.30	20.0	90.16	2:44
S3	100.00	16.0	100.00	4:31
S4	94.45	16.0	94.74	3:10
S5	98.81	18.5	94.12	2:46
S6	15.18	-	-	-
S7	93.61	16.7	98.61	3:48
S8	100.00	19.0	100.00	9:36
S9	95.46	16.3	91.67	2:28

C. Results

Table III shows the results of the experiment for all nine subjects. The classification accuracy of the BCI during the training phase is given as well as the average number of commands and the average classification accuracy during the runs. Also, the best time for navigating Rolland through the course is provided. Eight of nine subjects were able to navigate the wheelchair in a figure of eight.

The results were achieved using a segment length of $2s$ of acquired EEG-data to extract the SSVEP features and to classify the desired frequency. The feature extraction and classification step of the BCI was done every $0.1s$. To avoid that the same frequency is classified over and over again, because of the short time between two classifications, an idle period of $2s$ is considered during the signal processing of the EEG-data, i.e., after classification of a frequency, the earliest next classification of a frequency can be done after the idle period. Thus the subject got enough time to stop focusing attention to that stimulus. For calculation of the classification accuracy, only appropriate commands to fulfill the given task were considered as true positive classifications. To minimize the chance of false positive classifications, the behavior of the power in the corresponding frequency was observed in a range of $0.5s$ before and $0.5s$ after the classification of a command. If the power showed a significant behavior (i.e. continuous increase and decrease) over that period, that

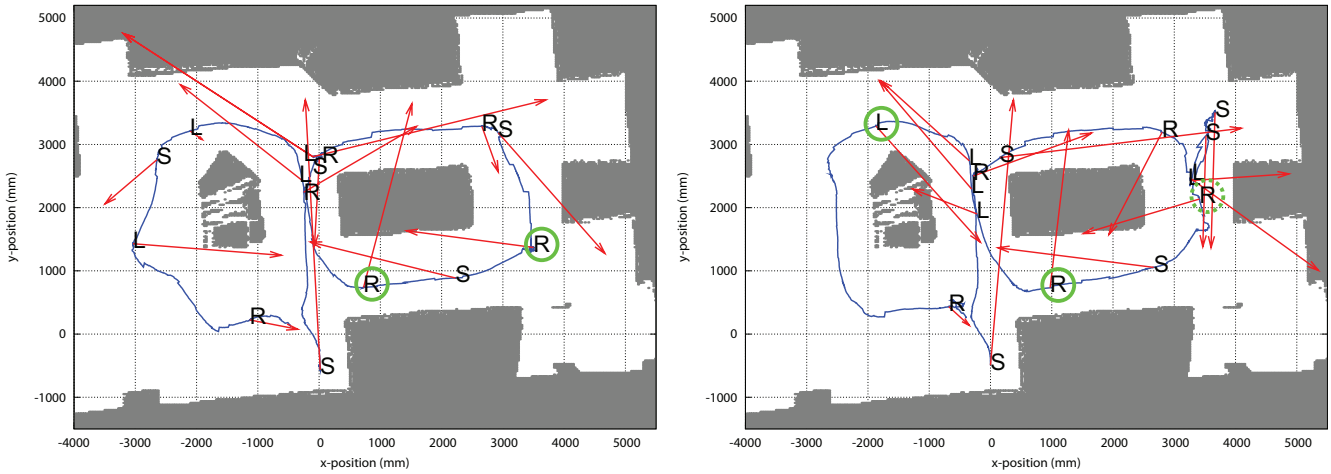

(a) subject S1, run 2

(b) subject S2, run 3

Fig. 5. Exemplary plots of trajectories as driven by two test persons within the scope of our pilot study. The experimental setup (cf. Section VII) asked nine subjects to drive a figure of eight within the depicted environment, starting with a clockwise movement from position $S = (0, 0)$, and finishing with a counter-clockwise movement nearby S. The paths printed as solid lines are given by an estimation of the GMapping localizer (cf. Subsection VII-B), and annotated by arrows based at the position of the wheelchair when receiving a new qualitative directional command coming from the BCI. The commands received are indicated by bold letters (*S=straight ahead, R=right, B=backwards, L=left*). Please note that arrowheads describe the resulting local navigation targets (cf. Section V) in odometry-coordinates.

command is considered as a true positive classification.

D. Discussion & Conclusion

During the training phase, eight of nine subjects showed good classification results of the desired frequency. The minimum classification accuracy was 93.61% (subject S7) during wheelchair movement. It seems that a stressful situation (subject is sitting in a moving wheelchair) does not affect the SSVEP response of that subject significantly. The range of the classification accuracy during the navigation task is quite similar to that during the training phase. For eight subjects, classification errors were mainly characterized as too many classifications of the same frequency the subject is attending to. An explanation is that some subjects showed a very high SSVEP response for the stimulus frequencies. If the signal processing analyzes the recent $2s$ of the acquired data every 0.1s, the power calculated is even quite high for some classification steps after the subject stopped focusing attention to the stimulus, because of the high SSVEP response. In future experiments, this can be avoided by using individual idle periods for subjects with high power in the stimulus frequencies over a long time, or by using shorter segment lengths (but this typically affects the classification accuracy more significantly). Only for a single subject (subject S6), the BCI was not able to classify the desired frequency accurately. But this corresponds to the percentage of BCI illiteracy reported in [35]. Another important issue is that all subjects, for who an SSVEP response could be obtained accurately, were able to navigate the wheelchair quite well after a minimal training phase (not more than 10 minutes) independent of their level of experience in BCI experiments. Those subjects were even able to correct wrong interpretations of a given command.

From the perspective of navigation, a major issue is the desired correspondence between the calculated, and the user-intended target position. Although general results indicate good performance of the algorithms involved, there exist situations in which the approach selected returns inadequate solutions. Considering the estimated positions of some commands given at locations that are marked by a solid circle in Fig. 5(a) - 5(b), it becomes obvious that the interpretation of the corresponding commands is not intuitive here. This behavior is due to the leading path-selection mechanism described in Section V that favors paths the final nodes of which fit closely to the commanded direction. When the Voronoi graph now includes paths that lead to currently unobservable but still mapped regions, targets may be chosen that do not correspond to the user's anticipation. With the path-selection scheme described in second place in Section V, the described problems vanish. The critical drawback that leaves this approach to work only under a perfect world assumption is that it is highly prone to topological changes in the Voronoi graph, as induced by sensor noise.

A second situation in which the navigational approach applied did not answer the expectations of the volunteers is exemplarily highlighted in Fig. 5(b) by a dashed circle around the place of a given BCI-command. The depicted case is designated by a target position that is located at the border to a region that was unobserved at the time of computation. While approaching the selected target, new sensor measurements revealed it to be located completely on the border to an occupied region. A following stop maneuver that was initiated by the downstream NDN module irritated the participant of the study, i.e. he/she had to give a new command shortly after the aborted one. Although this behavior does not meet everyday usability requirements, our current approach of canceling a target request by the NDN module, because of an appearing obstacle that blocks the goal location, seems justified. As a reason for this we refer

to the reduced complexity of interactions between the path selecting and executing modules.

VIII. ACKNOWLEDGMENTS

The authors would like to thank B. Gersdorf for the technical setup of the smart wheelchair platform Rolland. Further acknowledgements go to U. Frese for his support with the implementation and extension of the NDN-approach.

REFERENCES

[1] A. Lankenau and T. Röfer, "Smart wheelchairs - state of the art in an emerging market," *Künstliche Intelligenz. Schwerpunkt Autonome Mobile Systeme*, no. 4, pp. 37–39, 2000.

[2] R. C. Simpson, "Smart wheelchairs: A literature review." *Journal of Rehabilitation Research & Development*, vol. 42, no. 4, pp. 423–436, 2005.

[3] R. Simpson and S. Levine, "Voice control of a powered wheelchair," *IEEE Transactions on Neural Systems and Rehabilitation Engineering*, vol. 10, no. 2, pp. 122–125, June 2002.

[4] C. Mandel, U. Frese, and T. Röfer, "Robot Navigation based on the Mapping of Coarse Qualitative Route Descriptions to Route Graphs," in *Proceedings of the IEEE/RSJ Intl. Conference on Intelligent Robots and Systems (IROS 2006)*. IEEE Xplore, 2006, pp. 205–210.

[5] M. Bureau, J. Azkoitia, G. Ezmendi, I. Manterola, and H. Zabaleta, "Non-invasive, wireless and universal interface for the control of peripheral devices by means of head movements," in *Proceedings of the 10th IEEE Intl. Conf. on Rehabilitation Robotics (ICORR)*, 2007.

[6] C. Mandel, T. Röfer, and U. Frese, "Applying a 3DOF Orientation Tracker as a Human-Robot Interface for Autonomous Wheelchairs," in *Proceedings of the IEEE 10th International Conference on Rehabilitation Robotics (ICORR 2007)*. IEEE Xplore, 2007.

[7] B. Z. Allison, E. W. Wolpaw, and J. R. Wolpaw, "Brain-computer interface systems: progress and prospects," *Expert Review of Medical Devices*, vol. 4, no. 4, pp. 463–474, 2007.

[8] E. Donchin, K. M. Spencer, and R. Wijesinghe, "The Mental Prosthesis: Assessing the Speed of a P300-Based Brain-Computer Interface," *IEEE Trans. on Rehabilitation Engineering*, vol. 8, no. 2, pp. 174–179, 2000.

[9] B. Blankertz, G. Dornhege, M. Krauledat, M. Schröder, J. Williamson, R. Murray-Smith, and K.-R. Müller, "The berlin brain-computer interface presents the novel mental typewriter Hex-o-Spell," in *Proceedings of the 3rd International Brain-Computer Interface Workshop and Training Course*. Verlag der Technischen Universität Graz, 2006.

[10] T. Lüth, D. Ojdanic, O. Friman, O. Prenzel, and A. Gräser, "Low level control in a semi-autonomous rehabilitation robotic system via a Brain-Computer Interface," *10th Int. Conf. on Rehab. Robotics (ICORR)*, pp. 721–728, 2007.

[11] G. R. Müller-Putz and G. Pfurtscheller, "Control of an Electrical Prosthesis With an SSVEP-Based BCI," *IEEE Trans. on Biomed. Eng.*, vol. 55, no. 1, pp. 361–364, 2008.

[12] C. Guger, C. Holzner, C. Grönegress, G. Edlinger, and M. Slater, "Control of a smart home with a brain-computer interface," in *Proceedings of the 4th International Brain-Computer Interface Workshop and Training Course*, 2008, pp. 339–342.

[13] B. Rebsamen, E. Burdet, C. Guan, C. L. Teo, Q. Zeng, M. Ang, and C. Laugier, "Controlling a wheelchair using a BCI with low information transfer rate," *10th Int. Conf. on Rehab. Robotics (ICORR)*, pp. 1003–1008, 2007.

[14] E. Lew, M. Nuttin, P. Ferrez, A. Degeest, A. Buttfield, G. Vanacker, and J. del R. Millan, "Non-invasive brain computer interface for mental control of a simulated wheelchair," *Proc. of the 3rd Int. Brain-Computer Interface Workshop & Training Course*, 2006.

[15] M. Cheng, X. Gao, S. Gao, and D. Xu, "Design and Implementation of a Brain-Computer Interface With High Transfer Rates," *IEEE Transactions on Biomedical Engineering*, vol. 49, no. 10, pp. 1181–1186, 2002.

[16] T. Röfer, J. Brose, D. Göhring, M. Jüngel, T. Laue, and M. Risler, "Germanteam 2007," in *RoboCup 2007: Robot Soccer World Cup XI Preproceedings*, U. Visser, F. Ribeiro, T. Ohashi, and F. Dellaert, Eds. RoboCup Federation, 2007.

[17] D. Regan, *Human Brain Electrophysiology: Evoked Potentials and Evoked Magnetic Fields in Science and Medicine*. New York: Elsevier, 1989.

[18] G. Burkitt, R. Silberstein, P. Cadusch, and A. Wood, "Steady-state visual evoked potentials and travelling waves," *Clinical Neurophysiology*, vol. 111, no. 2, pp. 246–258, 2000.

[19] C. S. Herrmann, "Human EEG responses to 1-100 hz flicker: resonance phenomena in visual cortex and their potential correlation to cognitive phenomena," *Exp. Brain Res.*, vol. 137, no. 3–4, pp. 346–353, 2001.

[20] O. Friman, I. Volosyak, and A. Gräser, "Multiple channel detection of steady-state visual evoked potentials for brain-computer interfaces," *IEEE Trans. on Biomedical Engineering*, vol. 54, no. 4, pp. 742–750, 2007.

[21] D. Valbuena, M. Cyriacks, O. Friman, I. Volosyak, and A. Gräser, "Brain-computer interface for high-level control of rehabilitation robotic systems," *10th International Conference on Rehabilitation Robotics*, pp. 619–625, 2007.

[22] O. Friman, T. Lüth, I. Volosyak, and A. Gräser, "Spelling with Steady-State Visual Evoked Potentials," *3rd International IEEE/EMBS Conference on Neural Engineering*, pp. 354–357, 2007.

[23] A. Elfes, "Occupancy Grids: A Probabilistic Framework for Robot Perception and Navigation," Ph.D. dissertation, Carnegie-Mellon University, 1989.

[24] M. Gavrilova and M. Alsuwaiyel, "Two algorithms for Computing the Euclidean Distance Transform," *International Journal of Image and Graphics*, vol. 1, no. 4, pp. 635–645, 2001.

[25] B. Krieg-Brückner, U. Frese, K. Lüttich, C. Mandel, T. Mossakowski, and R. Ross, "Specification of an Ontology for Route Graphs," in *Spatial Cognition IV*, ser. Lecture Notes in Artificial Intelligence, C. Freksa, M. Knauff, B. Krieg-Brückner, B. Nebel, and T. Barkowsky, Eds. Springer-Verlag, 2005, vol. 3343, pp. 390–412.

[26] H. Shi and B. Krieg-Brückner, "Modelling route instructions for robust human-robot interaction on navigation tasks," *International Journal of Software and Informatics*, vol. 2, no. 1, pp. 33–60, 2008.

[27] P. Hart, N. Nilsson, and B. Raphael, "A formal basis for the heuristic determinationof minimum cost paths," *Transactions on Systems Science and Cybernetics, IEEE*, vol. 4, no. 2, pp. 100–107, 1968.

[28] B. Graimann, B. Allison, C. Mandel, T. Lüth, D. Valbuena, and A. Gräser, *Robust Intelligent Systems*. Springer Verlag, 2008, ch. Non-invasive Brain-Computer Interfaces for Semi-Autonomous Assistive Devices, pp. 113–138.

[29] J. Minguez and L. Montano, "Nearness diagram (nd) navigation: Collision avoidance in troublesome scenarios," *IEEE Transactions on Robotics and Automation*, vol. 20, no. 1, 02 2004.

[30] J. Minguez, J. Osuna, and L. Montano, "A divide and conquer strategy based on situations to achieve reactive collision avoidance in troublesome scenarios," in *Proceedings of the IEEE International Conference on Robotics and Automation (ICRA), 2004*, 2004.

[31] P. Kraetsch, "Entwicklung einer reaktiven steuerung für mobile roboter auf basis der nearness-diagram-methode für navigation in innenräumen," Master's thesis, Universität Bremen, 2007.

[32] G. E. Chatrian, E. Lettich, and P. L. Nelson, "Ten percent electrode system for topographic studies of spontaneous and evoked EEG activity," *Am. J. EEG Technol.*, vol. 25, pp. 83–92, 1985.

[33] "OpenSLAM web page," http://OpenSLAM.org/.

[34] G. Grisetti, C. Stachniss, and W. Burgard, "Improved techniques for grid mapping with rao-blackwellized particle filters," *IEEE Transactions on Robotics*, 2006.

[35] B. Allison, I. Volosyak, T. Lüth, D. Valbuena, I. Sugiarto, M. A. Spiegel, A. Teymourian, I. S. Condro, A. Brindusescu, K. Stenzel, H. Cecotti, and A. Gräser, "BCI Demographics: How many (and what kinds of) people can use an SSVEP BCI?" in *Proceedings of the 4th International Brain-Computer Interface Workshop and Training Course*, 2008, pp. 333–338.